

Simulation of hyper-velocity impact on double honeycomb sandwich panel and its staggered improvement with internal-structure model

Ping Liu · Yan Liu · Xiong Zhang

Received: 12 February 2015 / Accepted: 23 February 2015
© Springer Science+Business Media Dordrecht 2015

Abstract The double honeycomb sandwich panel, which was formed by inserting an intermediate facesheet into single honeycomb core, showed better capability than single honeycomb panel in shielding hyper-velocity impact from space debris. Shielding structures with double honeycomb cores are thoroughly investigated with material point method and point-based internal-structure model. The front honeycomb core and the rear honeycomb core are staggered to obtain better shielding effect. It is found that staggered double honeycomb cores can fragment the debris and lessen impact threats much more than original double honeycomb cores. The sizes of the holes on the rear facesheet are greatly reduced, and the panels are not perforated for some impact velocities. Staggered double honeycomb panels can be adopted as novel effective shielding structures for hyper-velocity impacts.

Keywords Double honeycomb cores · Hyper-velocity impact · Material point method · Internal-structure model · Energy absorption

1 Introduction

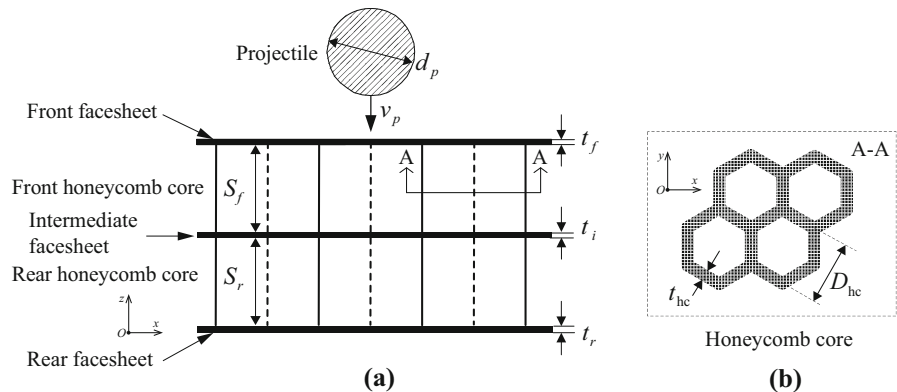
The design of shielding structure is very important for spacecraft due to the threats from space debris. As is one of the most widely-used structures, honeycomb sandwich panel subjected to hyper-velocity impact has been investigated by experiments (Lathrop and Sennett 1968; Taylor et al. 1999; Lambert et al. 2001) or numerical simulations (Taylor et al. 2003; Ryan et al. 2006). It is found that the honeycomb core has the effect of confining fragments within one to several core cells, called the channeling effect, which will decrease the shielding capability compared to common Whipple shielding structure.

However, wide use of honeycomb material in load-bearing components arouses interests in designing novel shielding structures made from honeycomb core. The sandwich panel with double honeycomb cores was proposed by Turner et al. (2001) by inserting another facesheet at the middle point of the honeycomb core. The sandwich panel with double honeycomb cores (referred as double honeycomb panel in the context) has higher ballistic limit than the one with single honeycomb core (referred as single honeycomb panel). Taylor et al. (2003) focused on numerical simulations of double honeycomb panel with different numerical methods. Performances of different methods were compared and commented, and the ballistic limit of the double honeycomb panel was given.

The difficulties of numerical simulation of hyper-velocity impact problems lie in extremely large

P. Liu · Y. Liu (✉) · X. Zhang
School of Aerospace Engineering, Tsinghua University,
Beijing 100084, People's Republic of China
e-mail: yan-liu@tsinghua.edu.cn

Fig. 1 The geometry of double honeycomb panel and the schematic diagram of the impact problem. **a** The front view. **b** The top view



deformation, crack propagation, and fragmentation such as debris cloud. Traditional finite element method (FEM) may suffer from mesh distortion and it is incapable of describing debris cloud correctly. Mesh-free particle methods (Zhang and Liu 2004), as an alternative to FEM, show great potential in analyzing hyper-velocity impact problems and studying hyper-velocity shielding structures (Taylor et al. 2003; Ryan et al. 2006; Liu et al. 2015).

Material point method (MPM) (Sulsky et al. 1994) is an efficient meshfree method (Ma et al. 2009; Zhang et al. 2013). The idea of MPM can be traced back to particle-in-cell method. One set of Lagrangian points carry history variables and move across another Eulerian background mesh in MPM. MPM possesses both the advantages of Lagrangian scheme and Eulerian scheme but overcome their shortcomings. Similar to other meshfree particle methods, MPM is very competitive in simulating problems of large deformation and fracture, because no mesh distortion exists and moving discontinuities can be modeled naturally. Successful applications include low-velocity impact (Sulsky and Schreyer 1996), dynamic fracture (Chen et al. 2002; Shen 2009), fluid–structure interaction (Lian et al. 2012, 2014), and high-velocity impacts (Huang et al. 2008; Gong et al. 2012; Liu et al. 2013).

In our previous work (Liu et al. 2015), the shielding properties of single honeycomb panel was investigated with point-based internal-structure model and MPM simulation. The detailed structures of honeycomb cores were built instead of using a smeared constitutive model and the interactions between cell walls and the projectile were explicitly simulated. The easiness to construct internal-structure model is attributed to the particle nature of MPM, which greatly simplifies the discretization refinement at the impacted area and

the discretization of the linkage area between honeycomb core and facesheets. The single-valued velocity field inherent in MPM ensures high efficiency dealing with contacts between honeycomb cell walls and the projectile and self-contacts of cell walls.

Based on our previous work on internal-structure simulation (Liu et al. 2015), we thoroughly investigate double honeycomb panel and its improved form by staggering the two layers of honeycomb cores. The staggered double honeycomb panels are presented to obtain better shielding performances and lessening channeling effect. Section 2 demonstrates the shielding structures as well as a brief introduction to the simulation method. Section 3 emphasizes on the shielding performance of different kinds of double honeycomb panels based on a series of simulation results. The paper is concluded in Sect. 4.

2 Shielding structures with honeycomb core and simulation method

2.1 Geometry of double honeycomb panel

Double honeycomb panel has an intermediate facesheet inserting at the middle point of the commonly-used single honeycomb panel, as shown in Fig. 1. The left part of Fig. 1 shows the front view, and the right part shows the in-plane A–A section (top view). t_f , t_i and t_r are the thicknesses of the front facesheet, the intermediate facesheet and the rear facesheet, respectively. S_f is the distance between the intermediate facesheet and the front facesheet, and S_r is the distance between the intermediate facesheet and the rear facesheet. The vertical solid line in the honeycomb core represents the protruding edge, and the vertical

Table 1 Model parameters of double honeycomb sandwich panel (Turner et al. 2001)

| Parameters | t_f (mm) | t_i (mm) | t_r (mm) | S_f (mm) | S_r (mm) | t_{hc} (mm) | D_{hc} (mm) | d_p (mm) |
|------------|------------|------------|------------|------------|------------|---------------|---------------|------------|
| Value | 0.4 | 0.4 | 0.4 | 17 | 17 | 0.178 | 4.76 | 2.0 |

dashed line denotes the recessed edge. t_{hc} is the thickness of cell wall, and D_{hc} is the incircle diameter of the hexagonal cell. A projectile impacts on the front facesheet normally. Projectile parameters include the diameter d_p and the impact velocity v_p . The model parameters are listed in Table 1.

2.2 Improvement of double honeycomb shielding structure

It is observed in both experiments and simulations that the honeycomb core can confine the projectile fragments in small regions, which is called the channeling effect. As the destroyed area is very limited, the fragments confined in the channel still have large impact energy to threat devices behind. The shielding capability of honeycomb panel should be improved by lessening the channeling effect and improving energy absorption of honeycomb core. Two improved structures based on double honeycomb cores are developed to eliminate the channeling effect by forcing the fragments to impact the cell walls of the honeycomb core.

Figure 2 shows top and front views of the four honeycomb sandwich structures investigated in this paper. The projectile is shown as a shadow-filled circle in the top view, but not shown in the front view. The upper right sub-figure shows a normal double honeycomb panel (abbreviated as DH panel). The upper left sub-figure is an equivalent single honeycomb panel without intermediate facesheet (abbreviated as ESH panel), whose front facesheet and rear facesheet are thickened by one half the thickness of the intermediate facesheet of DH panel. The masses of ESH panel and DH panel are same. Two new structures by staggering the rear honeycomb core are shown in bottom sub-figures. The lower left structure is constructed by staggering the rear honeycomb core in x -direction for one half cell, which will be abbreviated as XSDH panel. The lower right structure is constructed by staggering the rear honeycomb core in y -direction for one half cell, which will be abbreviated as YSDH panel. The projectile fragments will be further cut and spread by cell walls of the rear honeycomb core in XSDH and YSDH panels, so

that the shielding capability can be increased. The symmetry with respect to x -axis is invoked for ESH, DH and XSDH panels. Since the above symmetry does not exist for YSDH panel, a whole model is simulated for YSDH panel so that the four configurations can be compared in the same view angle.

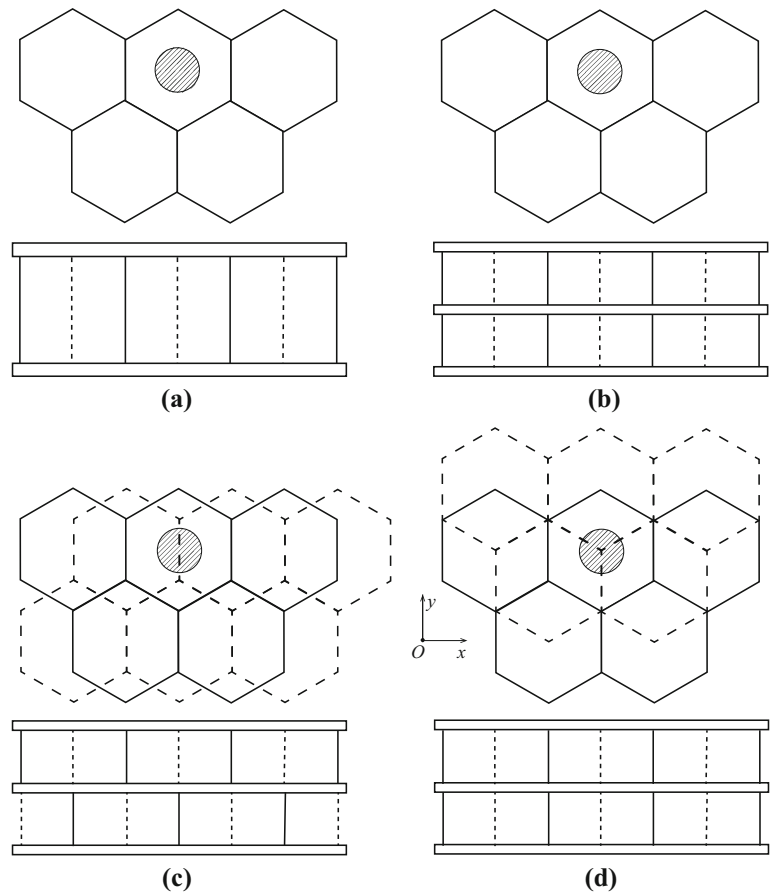
2.3 Brief introduction to simulation method

Both Lagrangian points and Eulerian background mesh are used in MPM. Lagrangian points trace history variables, such as stress, strain and energy. The background mesh is used to solve momentum equations and to calculate the spatial derivatives. At the beginning of each MPM step, a regular background mesh is established, and the history variables are mapped from Lagrangian points to background mesh nodes. In other words, Lagrangian points are bound to and deform with background mesh simultaneously inside each step. The momentum equations are solved on the background mesh. The variables on Lagrangian points are updated based on the increments on background mesh nodes. At the end of the step, the deformed background mesh is abandoned. For the next MPM step, regular background mesh is reproduced. As a result, Lagrangian points can overcome the challenge of tracing problems and convection term in Eulerian method. And Eulerian background mesh can guarantee valid element deformation and appropriate time step size which may be encounter difficulties for simulating large deformation with traditional Lagrangian meshed method.

The inherent contact algorithm in standard MPM is a non-slip contact, because single-valued velocity field is ensured (Sulsky et al. 1995). The influence of contact algorithm with friction was discussed with numerical experiments in Liu et al. (2015), and the friction coefficient was found to effect little on the final morphology in high-velocity impact.

The internal-structure model was established according to the method described in our previous work (Liu et al. 2015). Building point-type internal structure is very straightforward owing to the flexibility of

Fig. 2 Shielding structures based on single honeycomb core and double honeycomb cores. **a** ESH panel, **b** DH panel, **c** XSDH panel, **d** YSDH panel



arranging points without the requirement to link them to elements. The connection between facesheets and honeycomb cores does not require special consideration, either. It is also convenient for MPM to refine the model to improve local description and to show the details of the impact process. The internal-structure model for single honeycomb panel subjected to high-velocity impact have been thoroughly validated with experimental results (Liu et al. 2015). The same method is adopted for double honeycomb panels, and we focus on the shielding properties of different double honeycomb structures in this paper.

2.4 Material model

The facesheets are made of Al2024-T81, the honeycomb cores are made of Al5052, and the projectile is made of Al2017. All the materials are consistent with experiments in Turner et al. (2001). Johnson–Cook

strength model and Mie–Grüneisen equation of state (EOS) are combined to simulate the behavior of aluminum alloy under high pressure and high temperature. The material parameter values are the same as in Liu et al. (2015), where the parameter values were examined with experimental results and empirical formulas.

The Johnson–Cook strength model is for updating the deviatoric stress s_{ij} , and EOS is used to update the pressure p . The total stress $\sigma_{ij} = -p\delta_{ij} + s_{ij}$, where δ_{ij} is the Kronecker delta. The yield stress σ_y depends on the equivalent plastic strain ε^p , the strain rate $\dot{\varepsilon}$, and the temperature T in Johnson–Cook strength model (Johnson and Cook 1983),

$$\sigma_y = (A + B(\varepsilon^p)^n)(1 + C \ln \dot{\varepsilon}^*)(1 - T^{*m}) \quad (1)$$

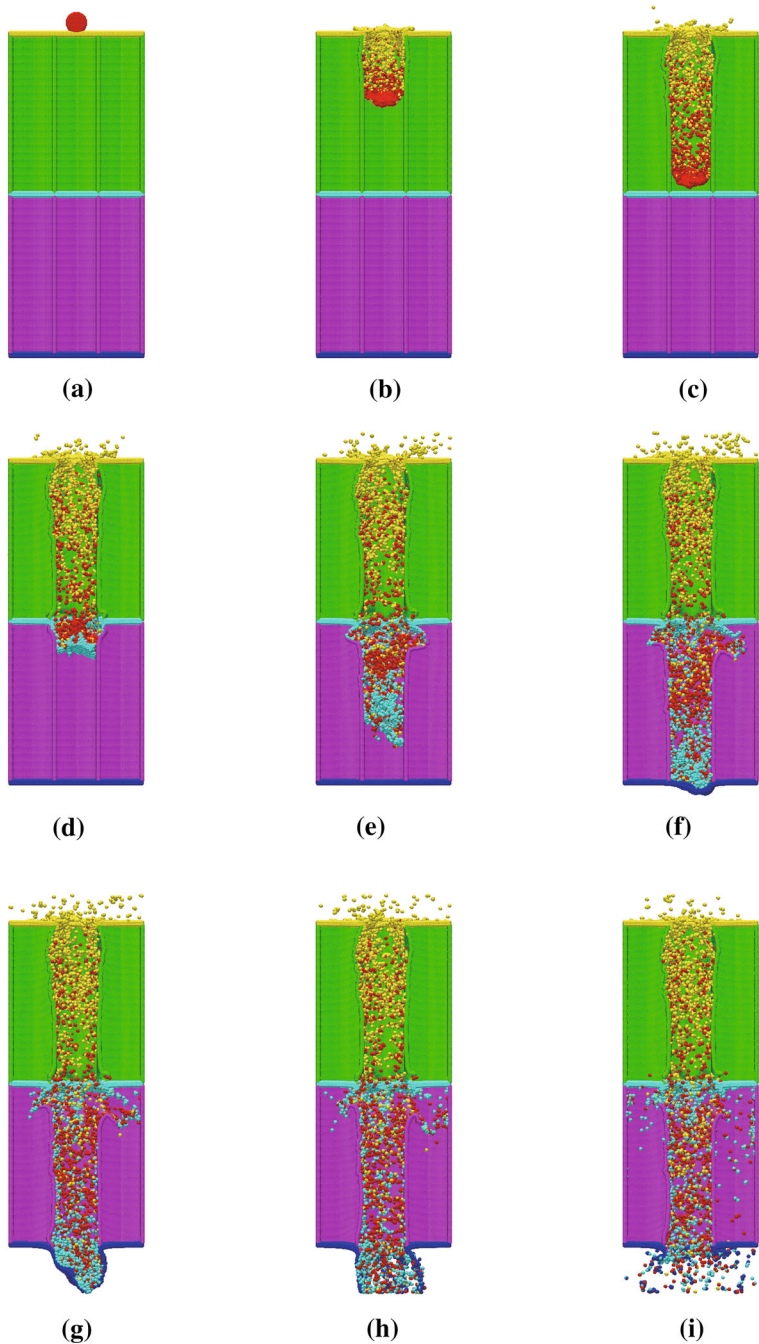
where A, B, n, c, m are material parameters. $\dot{\varepsilon}^* = \dot{\varepsilon}/\dot{\varepsilon}_0$ is the dimensionless equivalent strain rate with the reference strain rate $\dot{\varepsilon}_0 = 1.0 \text{ s}^{-1}$. The homologous

temperature $T^* = (T - T_{\text{room}})/(T_{\text{melt}} - T_{\text{room}})$. T_{room} and T_{melt} are the room temperature and the melting temperature, respectively. A damage model is incorporated to depict material failure of honeycomb core. Facesheet and projectile materials fail when the principal tensile stress reaches the criterion value

σ_{max} . Failure model of principal stress can be used to approximately determine spalling failure, which is a common process in hyper-velocity impact.

Mie–Grüneisen EOS can describe well the variation of pressure inside metals when subjected to impact loading. The pressure in Mie–Grüneisen EOS

Fig. 3 Detailed impact process of DH panel. $v_p = 5 \text{ km/s}$. **a** $t = 0 \text{ } \mu\text{s}$, **b** $t = 2 \text{ } \mu\text{s}$, **c** $t = 4 \text{ } \mu\text{s}$, **d** $t = 6 \text{ } \mu\text{s}$, **e** $t = 10 \text{ } \mu\text{s}$, **f** $t = 14 \text{ } \mu\text{s}$, **g** $t = 18 \text{ } \mu\text{s}$, **h** $t = 22 \text{ } \mu\text{s}$, **i** $t = 50 \text{ } \mu\text{s}$



is calculated from the volumetric strain, the temperature and the internal energy as

$$p = p_H \left(1 - \frac{\gamma \mu}{2} \right) + \gamma_0 E_0 \tag{2}$$

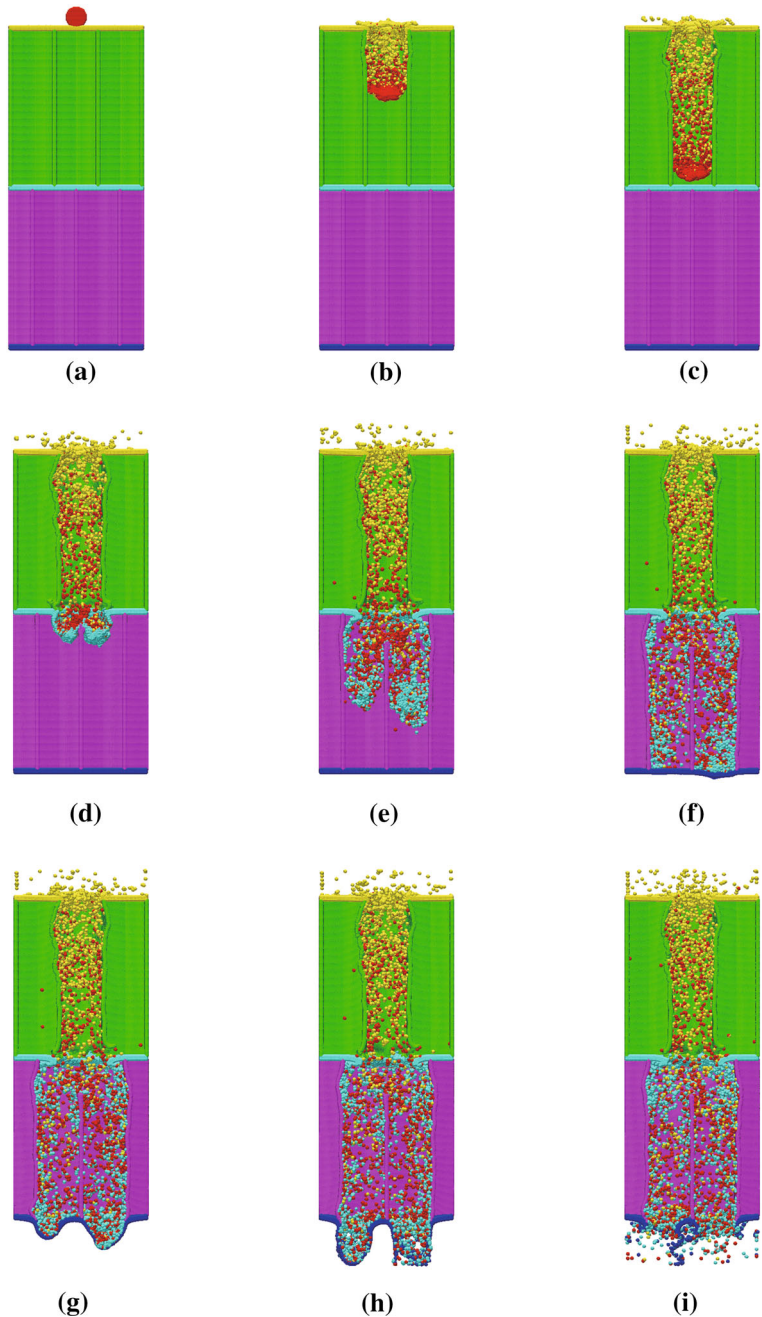
where γ is the Grüneisen parameter. The equation $\gamma_0 \rho_0 = \gamma \rho$ applies, where ρ is material density, and γ_0 and ρ_0 are respective values at initial state. The

volumetric strain $\mu = \rho / \rho_0 - 1$. E_0 is the initial specific internal energy. p_H is calculated by

$$p_H = \begin{cases} \frac{\rho_0 c_0 \mu (1 + \mu)}{[1 - (s - 1)\mu]^2} & \text{for } \mu \geq 0 \\ \rho_0 c_0 \mu & \text{for } \mu < 0 \end{cases} \tag{3}$$

where c_0 is the sound speed and s is a material parameter.

Fig. 4 Detailed impact process of XSDH panel. $v_p = 5$ km/s. **a** $t = 0 \mu\text{s}$, **b** $t = 2 \mu\text{s}$, **c** $t = 4 \mu\text{s}$, **d** $t = 6 \mu\text{s}$, **e** $t = 10 \mu\text{s}$, **f** $t = 14 \mu\text{s}$, **g** $t = 18 \mu\text{s}$, **h** $t = 22 \mu\text{s}$, **i** $t = 50 \mu\text{s}$

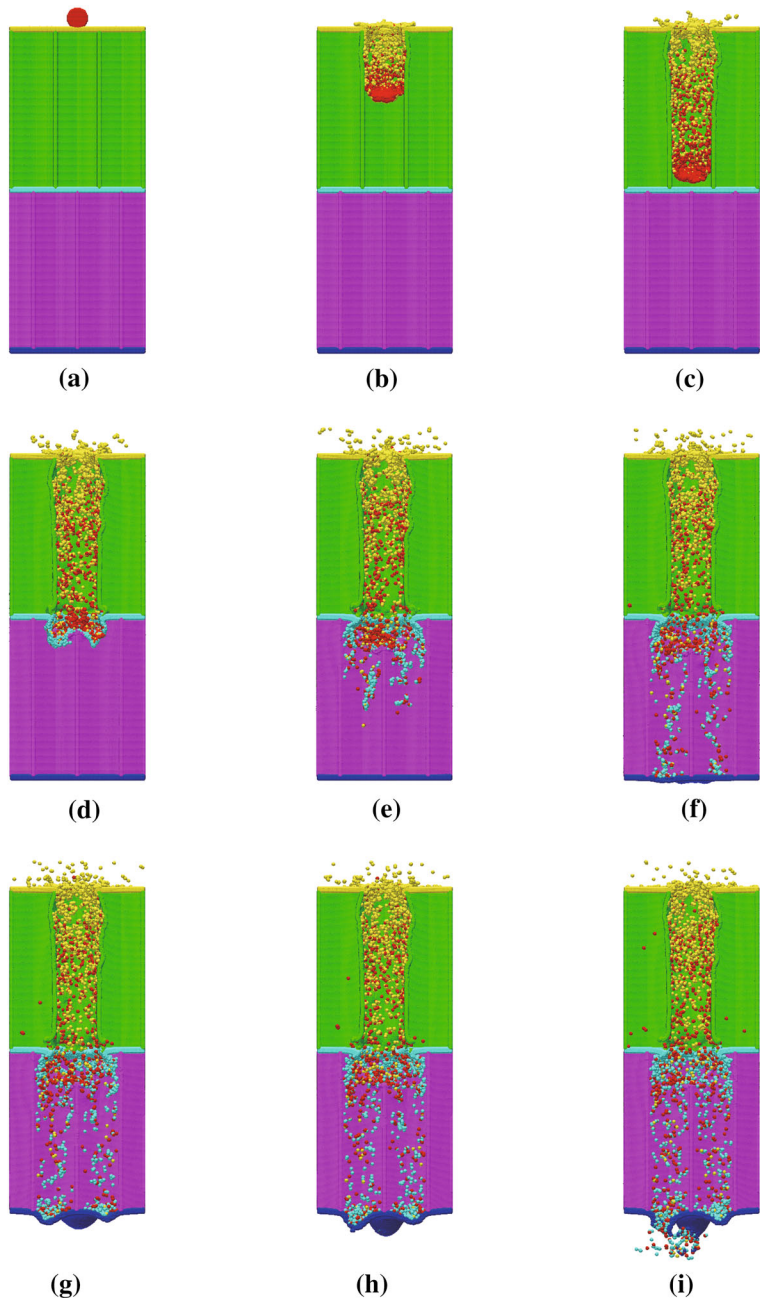


3 Results analysis and shielding capability of double honeycomb structures

3.1 Detailed impact processes of different shielding structures

Firstly, the impact and perforation processes of different shielding structures are analyzed in detail

Fig. 5 Detailed impact process of YSDH panel. $v_p = 5$ km/s. **a** $t = 0$ μ s, **b** $t = 2$ μ s, **c** $t = 4$ μ s, **d** $t = 6$ μ s, **e** $t = 10$ μ s, **f** $t = 14$ μ s, **g** $t = 18$ μ s, **h** $t = 22$ μ s, **i** $t = 50$ μ s

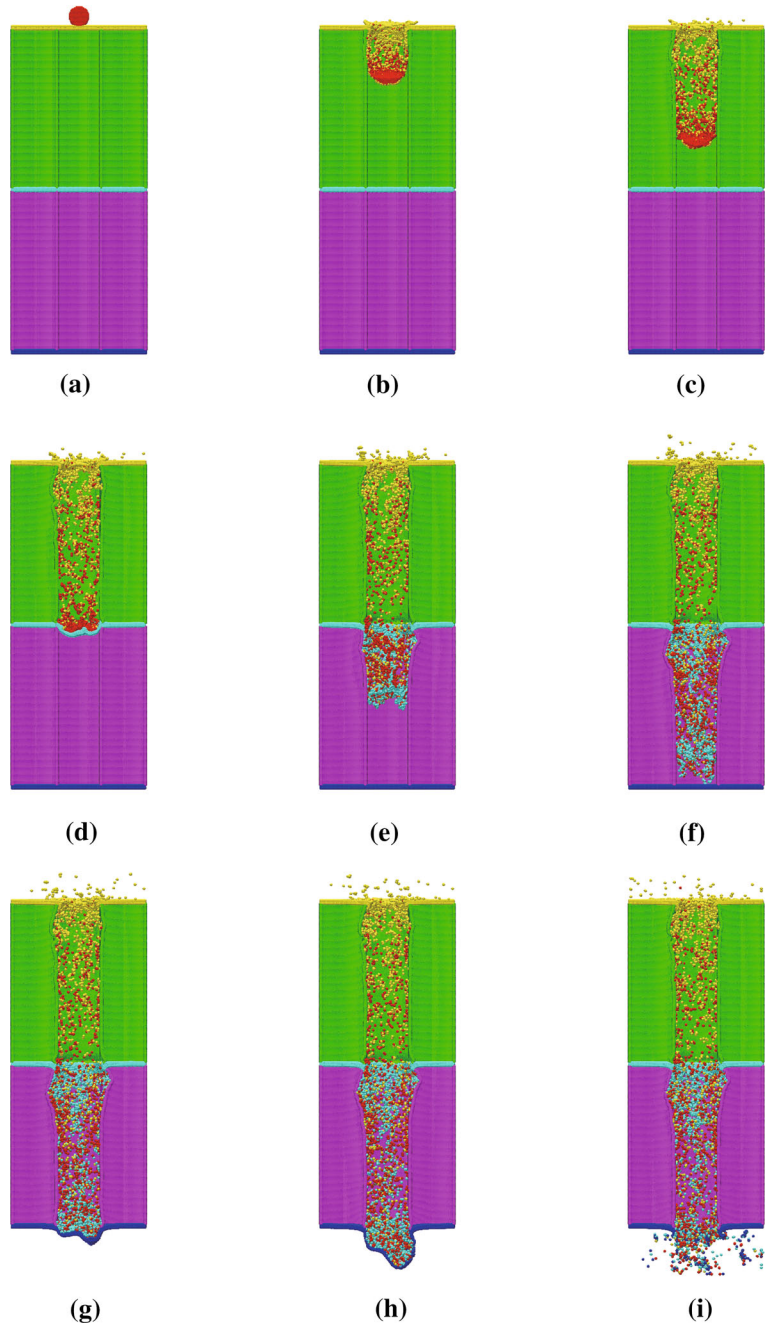


for the impact velocity 5 km/s. The detailed impact process of DH panel is shown in Fig. 3, and different components are displayed with different colors. Figure 3a–c shows the perforation of front facesheet. All the fragmented materials, including the projectile fragments and the failed material of front facesheet, are restricted in one honeycomb cell. The process is nearly the same as single honeycomb panel since the

intermediate plate, the rear honeycomb core, and the rear facesheet have negligible influences during the perforation of front facesheet. The front honeycomb core is also damaged, but large deformation region is only close to the front facesheet. When the fragmented materials strike on the intermediate facesheet, the intermediate facesheet also fails due to large residual

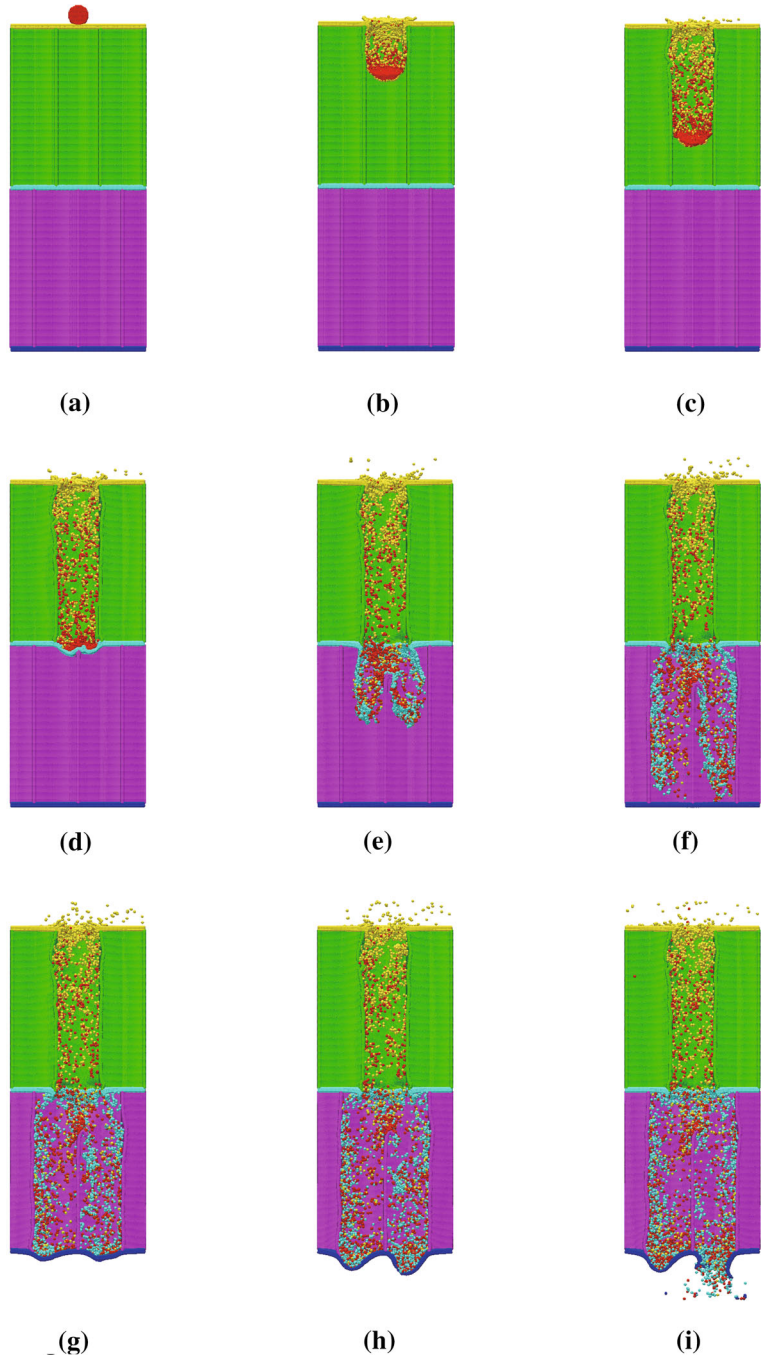
kinetic energy after first impact, as shown in Fig. 3d, e. The perforated area of the intermediate plate, however, is much larger than that of the front facesheet. Obvious perforation of the side wall of the rear honeycomb core can be seen at the intersection of the intermediate plate in Fig. 3e. The time for the fragmented materials traveling between the

Fig. 6 Detailed impact process of DH panel. $v_p = 4 \text{ km/s}$. **a** $t = 0 \text{ }\mu\text{s}$, **b** $t = 2 \text{ }\mu\text{s}$, **c** $t = 4 \text{ }\mu\text{s}$, **d** $t = 6 \text{ }\mu\text{s}$, **e** $t = 10 \text{ }\mu\text{s}$, **f** $t = 14 \text{ }\mu\text{s}$, **g** $t = 18 \text{ }\mu\text{s}$, **h** $t = 22 \text{ }\mu\text{s}$, **i** $t = 50 \text{ }\mu\text{s}$



intermediate and the rear facesheets is much longer than that between the front and the intermediate facesheets, which indicates that a large part of kinetic energy of the fragments has been absorbed by the impact with intermediate plate. Figure 3f–i shows the perforation of the rear facesheet and the formation of debris cloud.

Fig. 7 Detailed impact process of XSDH panel. $v_p = 4$ km/s. **a** $t = 0$ μ s, **b** $t = 2$ μ s, **c** $t = 4$ μ s, **d** $t = 6$ μ s, **e** $t = 10$ μ s, **f** $t = 14$ μ s, **g** $t = 18$ μ s, **h** $t = 22$ μ s, **i** $t = 50$ μ s



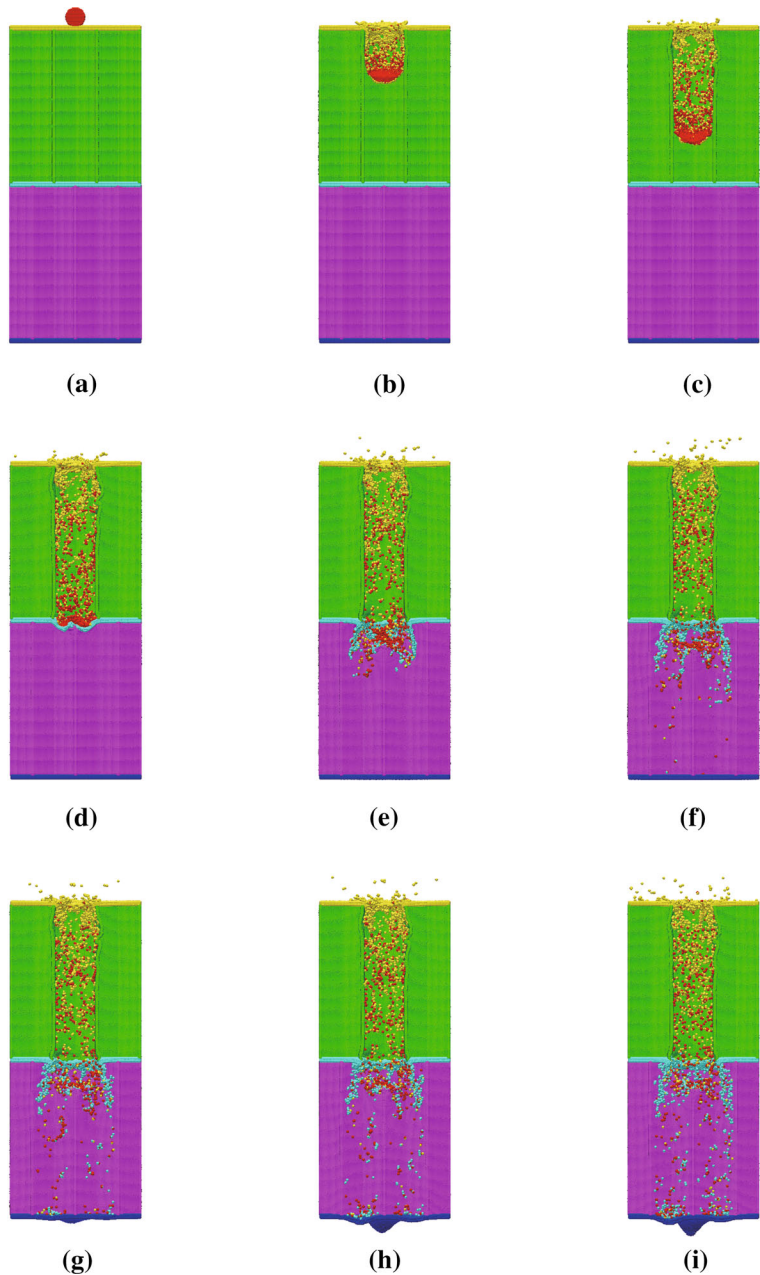
The detailed impact process of XSDH panel is shown in Fig. 4. As expected, the process perforating the front facesheet has negligible difference from that of original DH panel, since the impact is too transient for the supporting structures to respond. The differences can be found from Fig. 4d when the fragmented materials reach the intermediate facesheet. The

fragmented materials are further cut by the staggered cell walls of the rear honeycomb core and more impact energy is absorbed. Comparison of Figs. 3e and 4e indicates that the fragmented materials in XSDH panel are slower than those in original DH panel owing to more energy dissipation by the rear honeycomb core. All the fragments are limited in two cells of the rear honeycomb core. Though the remaining fragments

perforate the rear facesheet as two holes are formed in Fig. 4i, the hole diameters are obviously smaller than that in Fig. 3i.

The detailed impact process of YSDH panel is shown in Fig. 5. The intersection of the cell walls is struck directly by the fragments, as shown in Fig. 5d, so more energy can be absorbed than in XSDH panel. Figure 5e shows that the velocities (then the kinetic

Fig. 8 Detailed impact process of YSDH panel. $v_p = 4 \text{ km/s}$. **a** $t = 0 \text{ }\mu\text{s}$, **b** $t = 2 \text{ }\mu\text{s}$, **c** $t = 4 \text{ }\mu\text{s}$, **d** $t = 6 \text{ }\mu\text{s}$, **e** $t = 10 \text{ }\mu\text{s}$, **f** $t = 14 \text{ }\mu\text{s}$, **g** $t = 18 \text{ }\mu\text{s}$, **h** $t = 22 \text{ }\mu\text{s}$, **i** $t = 50 \text{ }\mu\text{s}$



energy) of the fragmented materials are much smaller than those in XSDH and DH panels when compared to Figs. 3e and 4e. The hole diameters of the rear facesheet are sharply decreased as shown in Fig. 5i.

Detailed impact processes of DH, XSDH, and YSDH panels under impact velocity 4 km/s are shown in Figs. 6, 7 and 8, respectively. Dynamical responses are similar to the case when $v_p = 5$ km/s. But YSDH panel has an obviously better shielding performance than the other two panels, because the rear facesheet is not perforated. XSDH panel also shows performance increase over traditional DH panel. Only one small perforation hole is observed in XSDH panel, and the

residual kinetic energy of the debris fragments is also greatly reduced.

3.2 Damages to the rear facesheet

Final morphologies of the rear facesheet of different shielding structures are compared in Figs. 9 and 10. When $v_p = 5$ km/s, all the structures are perforated, but the holes in XSDH and YSDH panels are much smaller than those in ESH and DH panels. When $v_p = 4$ km/s, much better shielding performances for XSDH and YSDH panels are demonstrated than DH and ESH panels. Only bulges but no perforation are

Fig. 9 Top view (a–d) and front view (e–h) of the rear facesheets in different honeycomb panels at $t = 50 \mu\text{s}$. $v_p = 5$ km/s. **a** ESH, **b** DH, **c** XSDH, **d** YSDH, **e** ESH, **f** DH, **g** XSDH, **h** YSDH

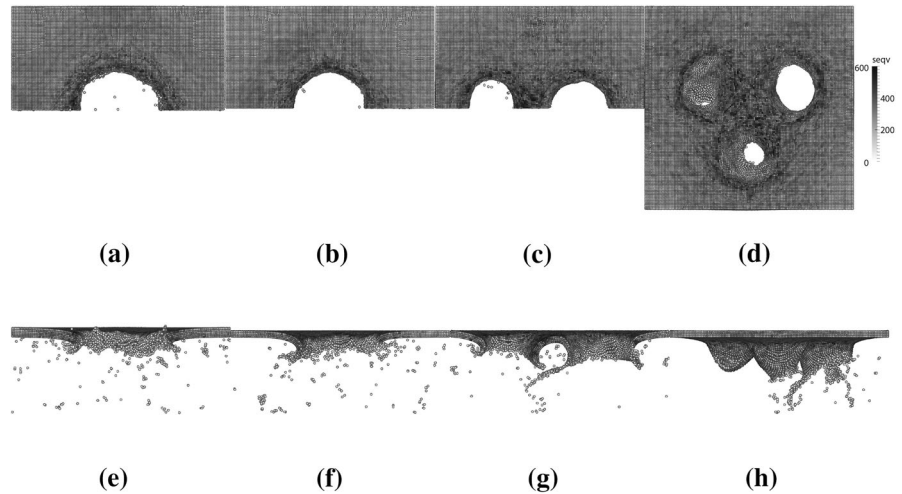
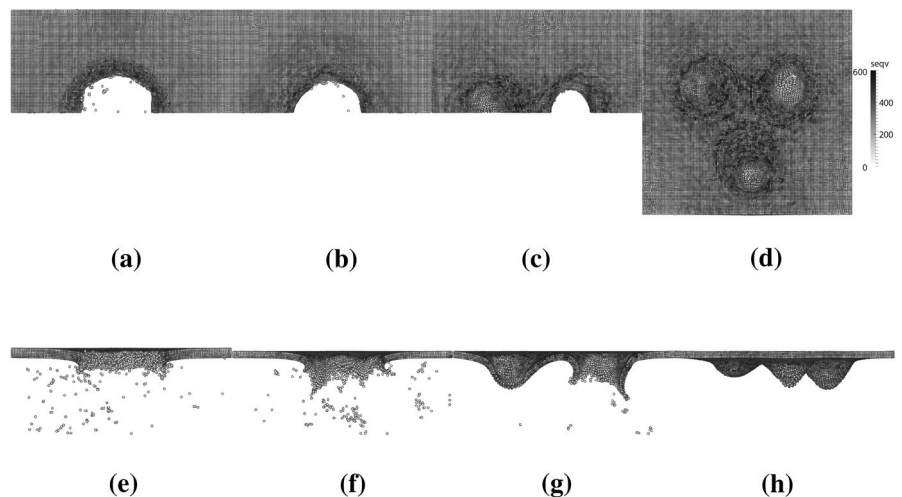


Fig. 10 Top view (a–d) and front view (e–h) of the rear facesheets in different honeycomb panels at $t = 50 \mu\text{s}$. $v_p = 4$ km/s. **a** ESH, **b** DH, **c** XSDH, **d** YSDH, **e** ESH, **f** DH, **g** XSDH, **h** YSDH



observed for YSDH panel, and the hole size of XSDH panel is very small.

Parameters measuring the damages to the rear facesheet are given in Table 2. Three more cases with $v_p = 3000, 3500,$ and 4500 m/s are listed besides the above two cases. D_{\max} is the diameter of the largest hole on the rear facesheet, which is calculated using the same measurement method as in our previous work (Liu et al. 2015). n_h is the number of the perforated holes. Some cases of XSDH and YSDH panel are not perforated but only some bulges can be found. The number of bulges is indicated as n_b . m_l is the dimensionless mass loss of the rear facesheet, which is defined as the lost mass during impact process divided by the initial mass.

It can be seen from Table 2 that DH panel can decrease hole size compared to ESH panel in most cases. This is because the projectile has been fragmented twice and the fragments spread larger range before they strike on the rear facesheet. The honeycomb cell walls also help more in DH panel than in ESH panel as they can absorb more energy during impact process of the intermediate facesheet.

The performance improvement is much more obvious for XSDH panel and YSDH panel. For $v_p = 3500$ m/s, both XSDH and YSDH panels are not perforated. The projectile of the velocity 4000 m/s does not perforate YSDH panel and only causes a very small hole on XSDH panel. Such good shielding results are achieved by only moving the rear honeycomb core for half cell size instead of adding extra mass. The honeycomb cores in XSDH and YSDH panels assist shielding more than in ESH and DH panels, because the fragments strike directly on the cell walls or the intersections of the rear honeycomb core rather than just scraping the cell walls or even pass through the honeycomb channel. The honeycomb core in XSDH and YSDH panels not only channels the fragments but also absorbs their kinetic energy.

The dimensionless mass loss m_l is introduced complimentary to D_{\max} and n_h to measure the overall damage to the rear facesheet. m_l takes into consideration the damages reflected by both perforation holes and bulges. In the case $v_p = 4000$ m/s and XSDH panel, for example, only one obvious hole is observed and another bulge without obvious perforation appears. Though D_{\max} in this case is about 67 % of that in DH panel and 58 % of that in ESH panel, m_l

Table 2 Damages to the rear facesheet

| Configuration | v_p (m/s) | n_h | n_b | D_{\max} (mm) | m_l |
|---------------|-------------|-------|-------|-----------------|--------|
| ESH | 3000 | 1 | 0 | 3.88 | 0.0424 |
| | 3500 | 1 | 0 | 5.15 | 0.0817 |
| | 4000 | 1 | 0 | 5.20 | 0.0845 |
| | 4500 | 1 | 0 | 5.23 | 0.0829 |
| | 5000 | 1 | 0 | 5.34 | 0.0870 |
| DH | 3000 | 1 | 0 | 4.72 | 0.0713 |
| | 3500 | 1 | 0 | 4.28 | 0.0371 |
| | 4000 | 1 | 0 | 4.46 | 0.0563 |
| | 4500 | 1 | 0 | 4.78 | 0.0595 |
| | 5000 | 1 | 0 | 4.99 | 0.0721 |
| XSDH | 3000 | 1 | 1 | 2.25 | 0.0082 |
| | 3500 | 0 | 2 | 0.00 | 0.0069 |
| | 4000 | 1 | 1 | 3.00 | 0.0132 |
| | 4500 | 2 | 0 | 3.70 | 0.0416 |
| | 5000 | 2 | 0 | 3.95 | 0.0375 |
| YSDH | 3000 | 1 | 2 | 2.15 | 0.0092 |
| | 3500 | 0 | 3 | 0.00 | 0.0069 |
| | 4000 | 0 | 3 | 0.00 | 0.0069 |
| | 4500 | 2 | 1 | 2.75 | 0.0095 |
| | 5000 | 3 | 0 | 3.10 | 0.0120 |

The bold values are used to emphasize that the corresponding cases are not perforated

is only 23 % of that in DH panel and 16 % of that in ESH panel showing that the damage in XSDH panel is greatly decreased. As shown in Table 2, most m_l s of YSDH panel are below 1 % and one order lower than those of DH and ESH panels, which again implies much better shielding effect.

Damages to DH, XSDH and YSDH structures reach minimum values at the velocity 3500 m/s. The reason may come from that factors dominating material failure behaviors are different when impact velocity changes, as literature (Seisson et al. 2014) pointed out. Plasticity may also play an important role around 3000 m/s, but its influence is decreased when the velocity further increases. And the effects of fragmentation and melting become very important.

3.3 Residual kinetic energy

The dimensionless residual kinetic energy, which is defined as the residual kinetic energy E_r^k divided by the initial kinetic energy E_0^k , are shown in Fig. 11. The

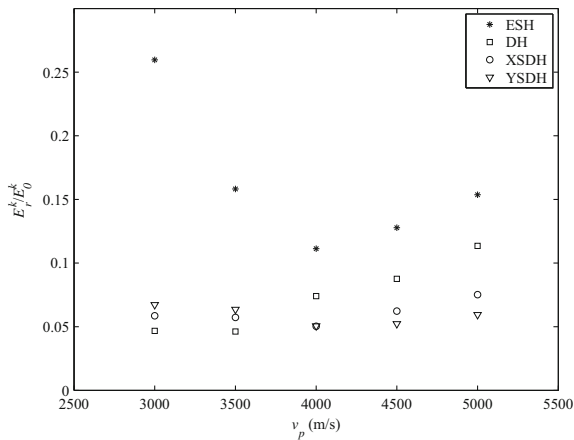


Fig. 11 Dimensionless residual kinetic energy

curves show that ESH panel has the most residual kinetic energy. The other three double honeycomb configurations have much better shielding performance. The residual kinetic energy is not zero for XSDH and YSDH panels when $v_p = 3500$ m/s though the two panels are not perforated, which is due to the kinetic energy carried by the fragments splashed backward. When the velocity is beyond 3500 m/s, the residual kinetic energies of XSDH panel and YSDH panel are obviously less than that of DH panel.

4 Conclusion

Shielding performances of original double honeycomb sandwich panel and two improved shielding structures are investigated in detail. The two improved structures are constructed by staggering the front and the rear honeycomb cores to enforce the projectile to impact on the honeycomb cell walls during shielding hyper-velocity impact. Internal structure models are built for all the sandwich panels, and all the impact processes are simulated with meshfree material point method.

Hole sizes, mass losses, and the residual kinetic energy are analyzed for all the shielding structures. All the double honeycomb configurations show better shielding ability than single honeycomb structure. The two staggered double honeycomb panels, denoted as XSDH panel and YSDH panel, demonstrate much better shielding performances against hyper-velocity impact. YSDH panels are not perforated when $v_p = 3500$ and 4000 m/s, and the hole sizes of XSDH and YSDH panels are greatly reduced compared to those

of original double honeycomb panel and single honeycomb panel. This is because impacts between honeycomb cell walls and debris fragments are strengthened by staggering honeycomb cores. The channeling effect is decreased as the debris fragments spread much larger range, and more impact energy is absorbed during impact with the honeycomb cores.

Further improvement of shielding structures based on honeycomb material will be the future work. Performance of structures with other functionality components, such as insulation layers, will also be investigated. The point-based model can deal with complex internal structure easily and efficiently, which is also ready to be extended to the analysis of more advanced materials from meso-scale simulation.

Acknowledgments Supported by National Natural Science Foundation of China (Grant No. 11472153) and Beijing Higher Education Young Elite Teacher Project (No. YETP0111).

References

- Chen, Z., Hu, W., Shen, L., Xin, X., Brannon, R.: An evaluation of the MPM for simulating dynamic failure with damage diffusion. *Eng. Fract. Mech.* **69**(17), 1873–1890 (2002)
- Gong, W., Liu, Y., Zhang, X., Ma, H.: Numerical investigation on dynamical response of aluminum foam subject to hyper-velocity impact with material point method. *CMES* **83**(5), 527–545 (2012)
- Huang, P., Zhang, X., Ma, S., Wang, H.: Shared memory OpenMP parallelization of explicit MPM and its application to hypervelocity impact. *CMES* **38**(2), 119–148 (2008)
- Johnson, G.R., Cook, W.H.: A constitutive model and data for metals subjected to large strains, high strain rates and high temperatures. In: *Proceedings of the 7th International Symposium on Ballistics*, vol. 21, pp. 541–547. The Hague, Netherlands: International Ballistics Committee (1983)
- Lambert, M., Schäfer, F.K., Geyer, T.: Impact damage on sandwich panels and multi-layer insulation. *Int. J. Impact Eng.* **26**(1), 369–380 (2001)
- Lathrop, B., Sennett, R.: Effects of hypervelocity impact on honeycomb structures. *J. Spacecr. Rockets* **5**(12), 1496–1497 (1968)
- Lian, Y.P., Liu, Y., Zhang, X.: Coupling of membrane element with material point method for fluid membrane interaction problems. *Int. J. Mech. Mater. Des.* **10**(2), 199–211 (2014)
- Lian, Y.P., Zhang, X., Liu, Y.: An adaptive finite element material point method and its application in extreme deformation problems. *Comput. Methods Appl. Mech. Eng.* **241–244**(1), 275–285 (2012)
- Liu, P., Liu, Y., Zhang, X.: Internal-structure-model based simulation research of shielding properties of honeycomb sandwich panel subjected to high-velocity impact. *Int. J. Impact Eng.* **77**, 120–133 (2015)

- Liu, P., Liu, Y., Zhang, X.: Investigation on high-velocity impact of micron particles using material point method. *Int. J. Impact Eng.* **75**, 241–254 (2015)
- Liu, Y., Wang, H.K., Zhang, X.: A multiscale framework for high-velocity impact process with combined material point method and molecular dynamics. *Int. J. Mech. Mater. Des.* **9**, 127–139 (2013)
- Ma, S., Zhang, X., Qiu, X.: Comparison study of MPM and SPH in modeling hypervelocity impact problems. *Int. J. Impact Eng.* **36**, 272–282 (2009)
- Ryan, S., Schaefer, F., Riedel, W.: Numerical simulation of hypervelocity impact on CFRP/Al hc sp spacecraft structures causing penetration and fragment ejection. *Int. J. Impact Eng.* **33**(1), 703–712 (2006)
- Seisson, G., Hébert, D., Hallo, L., Chevalier, J.M., Guillet, F., Berthe, L., Boustie, M.: Penetration and cratering experiments of graphite by 0.5-mm diameter steel spheres at various impact velocities. *Int. J. Impact Eng.* **70**, 14–20 (2014)
- Shen, L.: A rate-dependent damage/decohesion model for simulating glass fragmentation under impact using the material point method. *CMES* **14**(1), 23 (2009)
- Sulsky, D., Chen, Z., Schreyer, H.L.: A particle method for history-dependent materials. *Comput. Methods Appl. Mech. Eng.* **118**(1), 179–196 (1994)
- Sulsky, D., Schreyer, H.L.: Axisymmetric form of the material point method with applications to upsetting and Taylor impact problems. *Comput. Methods Appl. Mech. Eng.* **139**(1), 409–429 (1996)
- Sulsky, D., Zhou, S.J., Schreyer, H.L.: Application of a particle-in-cell method to solid mechanics. *Comput. Phys. Commun.* **87**(1), 236–252 (1995)
- Taylor, E., Herbert, M., Vaughan, B., McDonnell, J.: Hypervelocity impact on carbon fibre reinforced plastic/aluminium honeycomb: comparison with Whipple bumper shields. *Int. J. Impact Eng.* **23**(1), 883–893 (1999)
- Taylor, E.A., Glanville, J.P., Clegg, R.A., Turner, R.G.: Hypervelocity impact on spacecraft honeycomb: hydrocode simulation and damage laws. *Int. J. Impact Eng.* **29**(1), 691–702 (2003)
- Turner, R.J., Taylor, E.A., McDonnell, J.A.M., Stokes, H., Marriott, P., Wilkinson, J., Catling, D.J., Vignjevic, R., Berthoud, L., Lambert, M.: Cost effective honeycomb and multi-layer insulation debris shields for unmanned spacecraft. *Int. J. Impact Eng.* **26**(1), 785–796 (2001)
- Zhang, X., Lian, Y.P., Liu, Y., Zhou, X.: *Material Point Method*. Tsinghua University Press, Beijing (2013)
- Zhang, X., Liu, Y.: *Meshless Methods*. Tsinghua University Press, Beijing (2004)